Tuning the peak effect in the $Y_{1-x}Nd_xBa_2Cu_3O_{7-\delta}$ compound

D.M. Gokhfeld[a], D.A. Balaev[a,b], I.S. Yakimov[b], M.I. Petrov[a], S.V. Semenov[a,b,*]

[a] *Kirensky Institute of Physics, Federal Research Center KSC SB RAS, Akademgorodok 50, Krasnoyarsk 660036, Russia*
[b] *Siberian Federal University, Krasnoyarsk 660041 Russia*

ARTICLE INFO

ABSTRACT

Polycrystalline $Y_{1-x}Nd_xBa_2Cu_3O_{7-\delta}$ (x=0.02, 0.11, and 0.25) superconductors are synthesized. Nd atoms are uniformly distributed over grains. The magnetization loops of the samples have a pronounced second peak in a wide temperature range. The magnetization data are analyzed using the extended critical state model. It is found that the order-disorder transition of the vortex lattice is affected by doping with neodymium and temperature; the second-peak field and width decrease monotonically with increasing x value. The undoped polycrystalline $YBa_2Cu_3O_{7-\delta}$ compound is assumed to exhibit the peak effect in higher magnetic fields.

1. Introduction

The critical current of type-II superconductors is determined by the magnetic flux pinning. The capability of current transfer can be considerably improved by using artificial structural defects, which work as pinning centers [1–3]. The structural defects can be embedded by admixing, doping, or irradiation. Different defects enhance the pinning in different magnetic field ranges and can give rise to the peak effect [3,4]. The peak effect consists in a counterintuitive growth of the critical current in a certain magnetic field range, which is accompanied by a fishtail peculiarity, i.e. the second peak in the forward and reverse branches of the magnetization loop. The peak effect is attributed to transitions of the Abrikosov vortex lattice [5,6] or to a phase separation [7,8].

The second peak is observed in the magnetization loops of bulk $YBa_2Cu_3O_{7-\delta}$ single crystals [5,9], while in the polycrystalline $YBa_2Cu_3O_{7-\delta}$ compound the peak effect is difficult to observe [10]. On the contrary, the magnetization loops of granular Nd- and Eu-based 1-2-3 superconductors contain the pronounced second peak corresponding to magnetic field H weaker than 50 kOe at temperatures above 10 K [10–12].

It is well-known that the critical current in the $YBa_2Cu_3O_{7-\delta}$ compounds can be increased by chemical substitution of rare-earth elements for Y [13–19] or Ba [20,21]. In addition, the peak effect in $YBa_2Cu_3O_{7-\delta}$ can be induced by doping with Nd [4,13,22,23].

It was demonstrated in many works that the peak maximum shifts upon temperature variation. However, other ways of shifting the second peak have not been investigated. In the present work, we study the second peak evolution in the $Y_{1-x}Nd_xBa_2Cu_3O_{7-\delta}$ compounds where Y is partially replaced by Nd.

This article is organized as follows. The experimental techniques used are outlined in Section 2. Sample characterization, including XRD and SEM studies and $M(T)$ and $R(T)$ measurements, is described in Section 3. Section 4 presents magnetization loops and magnetic field dependences of the critical current densities and pinning force densities obtained in the framework of the Bean model. In Section 4, we analyze the magnetization loops using the extended critical state model [24–26].

2. Experimental

A series of optimally doped $Y_{1-x}Nd_xBa_2Cu_3O_{7-\delta}$ (x=0.02, 0.11, and 0.25) samples was synthesized by the solid-state reactions technique. X-ray powder diffraction (XRD) data were obtained using Shimadzu XRD-7000S diffractometer (CuKα radiation). The 2θ angle ranged from 5° to 70° with a step of 0.02°. Scanning electron microscopy (SEM) and energy dispersive spectrometry (EDS) investigations of the synthesized samples were carried out using Hitachi TM 3000 microscope. To perform the resistive measurements, parallelepiped samples about $1 \times 1 \times 8$ mm³ in size were cut from the synthesized pellets.

* Corresponding author at: Kirensky Institute of Physics, Federal Research Center KSC SB RAS, Akademgorodok 50, Krasnoyarsk 660036, Russia.
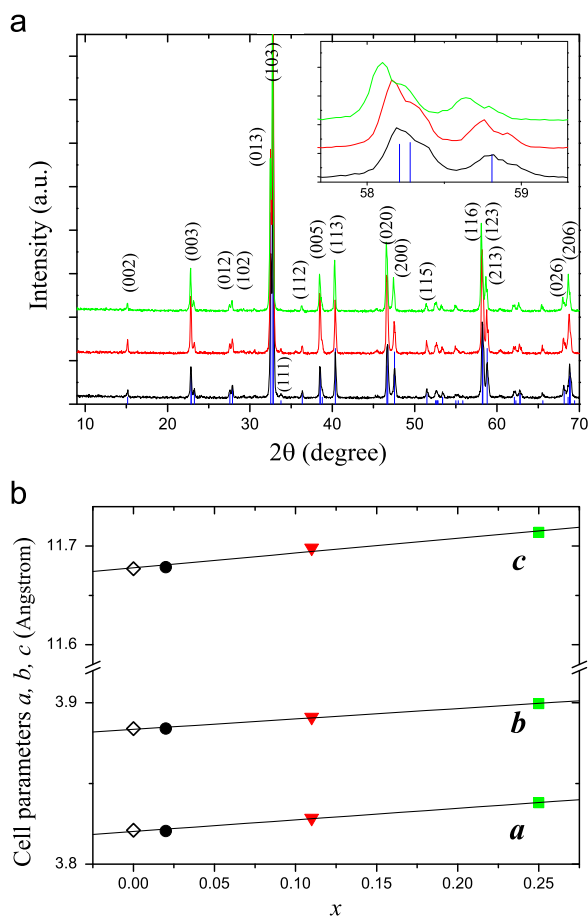 *E-mail address:* svsemenov@iph.krasn.ru (S.V. Semenov).

Fig. 1. (a) X-ray diffraction and (b) lattice parameters. For clarity, curves in Fig. 1a are shifted along the intensity axis. Lines in Fig. 1b are linear fits.

Temperature dependences of the resistivity $\rho(T)$ were measured by the four-probe method using the transport current of 1 mA. Magnetic measurements were performed using Quantum Design PPMS-6000 vibrating sample magnetometer.

3. Sample characterization

3.1. X-ray diffraction

Fig. 1a shows XRD patterns of the synthesized samples. Blue vertical marks in Fig. 1a indicate the PDF2 ICDD reference pattern #71-5184. All the peaks are seen to correspond to the peaks in a reference pattern of the orthorhombic $YBa_2Cu_3O_{7-\delta}$ material. No signs of other phases are observed. For the samples with $x=0.11$ and 0.25, the peaks are noticeably shifted to the left relative to their positions in the reference pattern (see Insert on Fig. 1a). This shift is proportional to the Nd content x.

The crystal lattice parameters were determined by the full-profile analysis using the DDM software [27]. Fig. 1b demonstrates the a, b, c parameters of the samples with different x; open circles show the parameters of the reference pattern ($YBa_2Cu_3O_{7-\delta}$). Where no error bars are shown, the errors are less than the symbol size. Each of the parameters a, b, and c grows linearly with x. The linear dependence of the a, b, and c values on x indicates that Nd is completely dissolved in the $Y_{1-x}Nd_xBa_2Cu_3O_{7-\delta}$ compound.

The XRD results conclude that the substitution of Nd with the larger atomic radius for Y causes the lattice expansion in $Y_{1-x}Nd_xBa_2Cu_3O_{7-\delta}$ compound.

3.2. Microstructure

SEM images of the samples are shown in Fig. 2a–c. The samples have the disordered granular structure. It can be seen that the samples with $x=0.11$ and 0.25 consist of coarser grains and are less porous than the sample with $x=0.02$. The average grain size is ~2.5 μm at $x=0.02$ and ~4 μm at $x=0.11$ and 0.25.

Fig. 2d shows a typical EDS image of the sample with $x=0.11$. Analysis of the elemental composition based on EDS map spectra showed that in all the samples the element contents correspond to the nominal chemical formula of the compound. The EDS images confirm the uniform distribution of Nd atoms over grains.

3.3. Critical temperature and $\rho(T)$ dependences

Fig. 3a shows temperature dependences of the magnetic moment $M(T)$ measured under zero field cooled (ZFC) and field cooled (FC) conditions in a magnetic field H of 10 Oe. The superconducting transition temperature T_c determined from these data is 92.5, 92.3, and 91.7 K for the samples with $x=0.02$, 0.11 and 0.25.

Fig. 3b shows the $\rho(T)$ dependences of the samples. At temperatures above T_c, these dependences exhibit the metal-like behavior typical of the YBCO system. The onset of the resistive transition corresponds to the T_c values obtained from the $M(T)$ dependence. The insert in Fig. 3b shows the enlarged resistive transition. The two-step $\rho(T)$ dependence near the superconducting transition is typical of granular high-T_c superconductors [28–30]. The sharp resistance drop corresponds to the superconducting transition of grains. The smooth part of the $\rho(T)$ dependence reflects the transition in the grain boundary subsystem, which can be presented as a Josephson junction network. For all the samples, the temperature range of the smooth part is 1.5–1.8 K. This indicates that the substitution of Nd for Y in $Y_{1-x}Nd_xBa_2Cu_3O_{7-\delta}$ almost does not change the intergrain (Josephson) coupling in the samples with $x \leq 0.25$.

4. Results and discussion

4.1. Magnetization loops

Fig. 4a–e show magnetic hysteresis loops for the $Y_{1-x}Nd_xBa_2Cu_3O_{7-\delta}$ samples in the temperature range of 4.2–80 K. The $M(H)$ dependences are tilted anticlockwise and their tilt increases with the Nd concentration x. In addition, in high fields the fishtail feature (the second peak) is observed.

The tilt of the magnetization loops is apparently related to the superposition of the magnetization hysteresis $M_S(H)$ of superconductive grains and additional paramagnetic magnetization $M_P(H)$ [11,12]. The additional paramagnetic magnetization can be taken into account from the high-field portion of the magnetization loop. This paramagnetic magnetization is expressed as $M_P(H)=NgJ\mu_B$ B_J $(gJ\mu_B\mu_0H/k_BT)$, where N is the number of magnetic ions per unit volume, μ_B is the Bohr magneton, k_B is the Boltzmann constant, g is the Lande g factor, J is the angular momentum quantum number, and B_J is Brillouin function. The N value is chosen to obtain the superconducting magnetization loops $M_S(H)=M(H)-M_P(H)$, which are not tilted in high fields H. One of the magnetization loops $M_S(H)$ without the paramagnetic contribution is presented in Fig. 4f. We found that the N value increases with
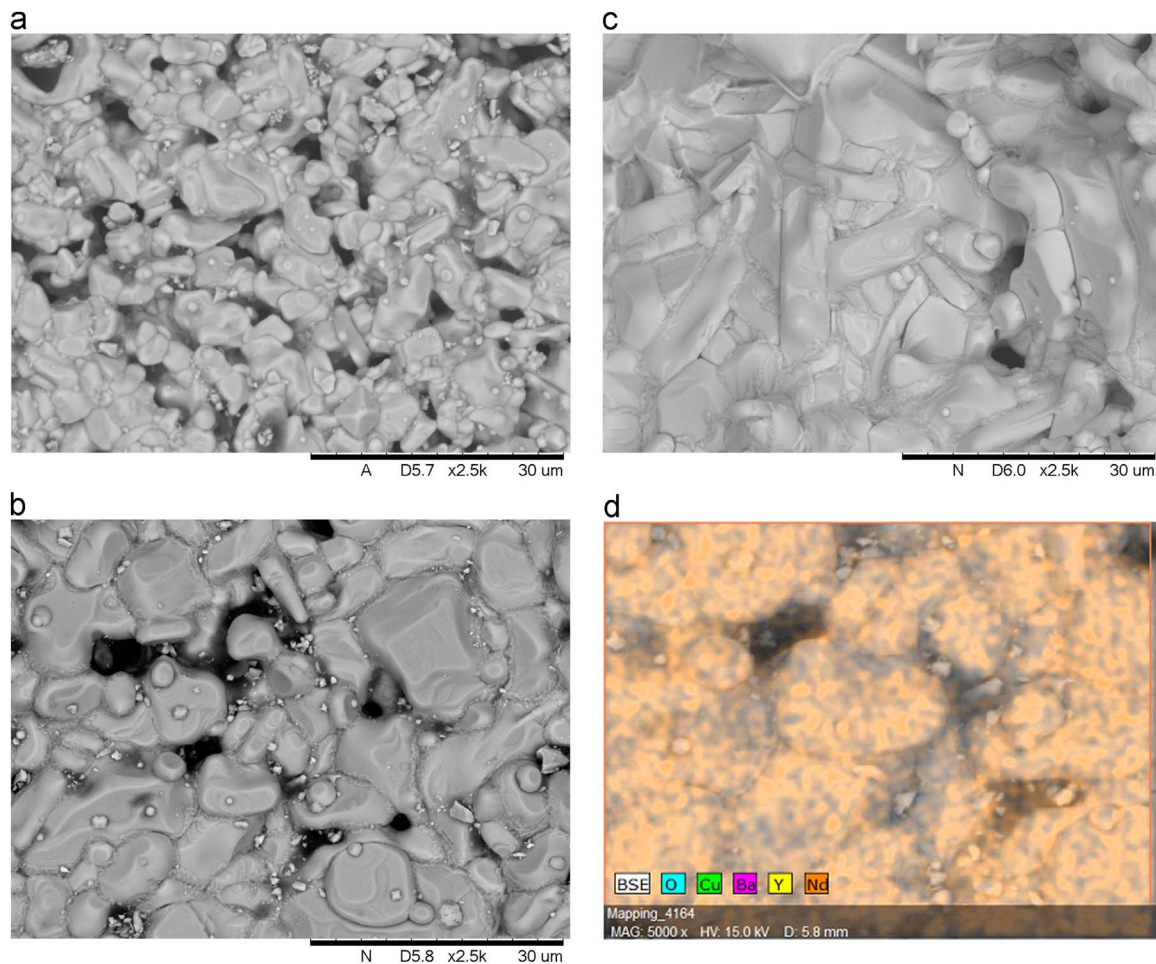
Fig. 2. SEM images of the samples with x=(a) 0.02, (b) 0.11, and (c) 0.25 and (d) EDS image of the sample with x=0.11.

temperature until T_c. The presented paramagnetic contribution to the $M(H)$ loop is the magnetization of Nd ions on the surface and in normal cores of the Abrikosov vortices [11]. At low temperatures, most Nd magnetic atoms are screened by the surface currents. As the temperature increases, both the vortex cores and the surface layer depth increase, so the larger number of Nd ions become unscreened.

4.2. Extended critical state model

The critical state model considers penetration of the magnetic flux in a superconducting sample [31]. The magnetic flux distribution depends on the critical current density and magnetization prehistory of the sample. The extended critical state model (ECSM) additionally takes into account the surface contribution to the magnetization [24–26]. The sample surface has the equilibrium magnetization independent of the magnetic prehistory. The surface layer is not involved in the transport current transfer [25,32], so the macroscopic critical current density depends on the surface layer depth l_s and the sample shape as

$$J_c(H) \cong j_c(H) \cdot [1 - 2l_s(H)/d]^n, \qquad (1)$$

where $j_c(H)$ is the local critical current density near the surface, d is the size of current circulation, and n is the parameter determined by the sample shape (n=3 for a long cylindrical sample and n=2 for a long plate parallel to H).

The incorrect J_c estimations are resulted due to a wrong choice of the size d. The d value can be equal to the sample radius, effective grain radius for the polycrystalline samples, or grain cluster size. The asymmetry of the magnetization loop relative to the axis M=0 depends also on l_s/d, which can be used to find d. The l_s value is no larger than the London penetration depth λ_0 [33]. The noticeable hysteresis asymmetry is observed when $2l_s/d > 0.1$, then we have $d < 20\lambda_0$.

The decreasing function for the unperturbed critical current density was defined as

$$J_c(H) = J_{c0} \frac{1 - |H/H_{c2}|^\alpha}{1 - |H/(h_1 H_{c2})|^\alpha} (1 - |H/H_{irr}|)^m \ \text{at} \ H \le H_{irr}$$

and

$$J_c(H) = 0 \ \text{at} \ H > H_{irr}, \qquad (2)$$

where α, m, and h_1 are the positive coefficients, $\alpha \le 1$, $m < n$, $h_1 < 1$, and $J_{c0}=j_c(0)[1-2l_s(0)/d]^n$. Expression (2) fits most experimental $J_c(H)$ curves without the peak effect.

The peak effect was described using the ECSM [8,34]. Here, we propose and justify a somewhat different approach, which will be described in more detail elsewhere. The fishtail feature can result from the transition between two states with different critical current densities $J_{c,1}(H)$ and $J_{c,2}(H)$. Such transitions is described by the Boltzmann expression [35].
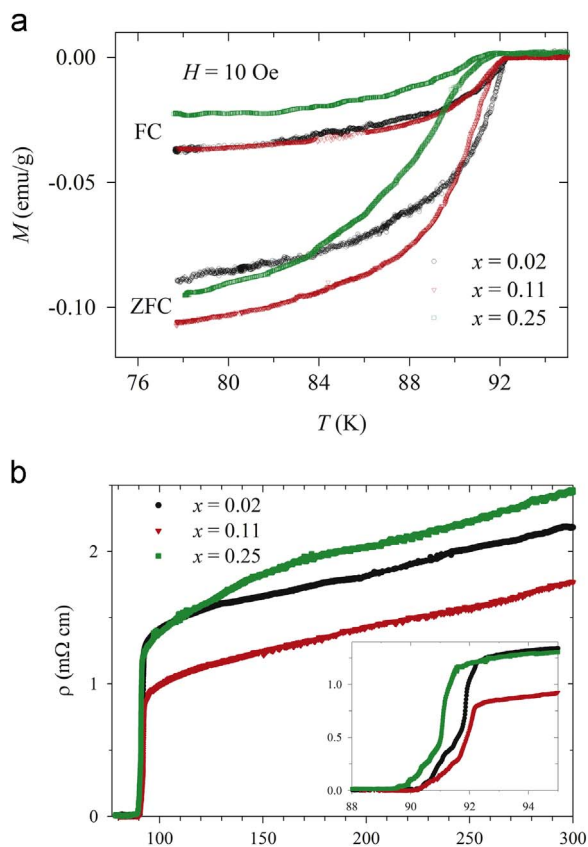
Fig. 3. Temperature dependences of (a) magnetization and (b) resistivity. Insert: resistive transition in the enlarged scale.

$$J_c(H) = J_{c,1}(H) + [J_{c,2}(H) - J_{c,1}(H)]S(H), \qquad (3)$$

where $S(H)$ is the logistic function. The fitting with the use of dependence (3) is complicated, because the zero-field critical current density $J_c(0)$ is the superposition of $J_{c,1}(0)$ and $J_{c,2}(0)$. For the sake of simplicity, we changed the logistic function by a sigmoid function, which is zero at $H=0$, and formula (3) becomes

$$J_c(H) \cong J_{c*}(H)\left(1 + \frac{A-1}{1 + |H_{tr}/H|^{H_{tr}/H_w}}\right), \qquad (4)$$

where $J_{c*}(H)$ is the decreasing function defined by (2), A is the peak height, H_{tr} is the center of the transition, and H_w is the transition width. Expression (4) is convenient to use, since $J_c(0)=J_{c*}(0)$ and $A=J_{c,2}(0)/J_{c*}(0)$.

4.3. Fitting the M(H) loops

We fitted all the measured magnetization loops using ECSM. For the investigated samples, the asymmetry of the $M_S(H)$ loops was used to estimate the d value (see Section 4.2). The circulation size d was found to be equal to the average grain size obtained from the SEM data (Section 3.2). It means that the estimated J_c values are the intragrain critical current density, which exceeds by far the intergrain one.

Fig. 4a–e (lines) show the fitting curves $M(H)=M_S(H)+M_P(H)$ together with experimental magnetization loops. A typical example of the fitting $M_S(H)$ and $M_P(H)$ curves is presented in Fig. 4f. The fitting parameters are given in Table 1. The center of the transition H_{tr} estimated from the fitting is about a half maximum pinning field H_{peak}

(see Section 4.4). The fitting demonstrates that at all temperatures the transition width H_w is about $H_{tr}/2$.

4.4. $J_c(H)$ and $F_p(H)$ dependences

Fig. 5a presents the $J_c(H)$ dependences (lines) computed using ECSM formula (4) with the parameters given in Table 1 at $T=60$ K. Points in Fig. 5a were obtained from the experimental $M(H)$ loops using the Bean formula $J_c(H)=3\Delta M/d$, where ΔM is the difference between the ascending and descending hysteresis branches and d is the characteristic current circulation size. As in the previous section, the d value was chosen to be the average grain size. It can be seen that the ECSM curves agree well with the $J_c(H)$ curves computed using the Bean formula.

The fishtail feature in the magnetization loops corresponds to the hump in the $J_c(H)$ dependences. The hump position depends on the x value. It can be seen in Fig. 5a that the hump shifts to the lower values as the x value increases.

The magnetic field dependences of the pinning force density F_p (Fig. 5b) are determined by $F_p(H)=\mu_0 H J_c(H)$. The maximum in the $F_p(H)$ dependence strongly depends on temperature. As the temperature increases, the maximum shifts to the left. In addition, the H_{peak} maximum position shifts to the lower values as the x value increases. At 60 and 80 K, for all the curves we have $H_{peak}\approx0.2\ H_{irr}$; therefore the pinning force scaling is apparently valid for these compounds, as for Nd-123 [11].

4.5. Tuning the peak effect by the Nd content variation

Fig. 6a and b summarize the effect of the Nd concentration on the H_{peak} peak position at different temperatures. In addition, the data for $x=1$ from [11] are plotted.

As was mentioned in Section 4.4, the H_{peak} peak position is governed by temperature. The maximum field H_{peak} and peak width H_w increase with decreasing temperature; i.e. the peak becomes smoother at low temperatures. As the temperature decreases from 80 to 4.2 K, the peak maximum H_{peak} shifts from 0.8–1 to 35–42 T (Fig. 6a). At $T=80$ K, the peak height A drastically decreases. Thus, the peak effect is difficult to observe at low temperatures, where the peak is very wide, and near T_c, where it becomes small.

The Nd concentration affects also the value of H_{peak}. In the investigated x range from 0.02 to 0.25, the peak position monotonically decreases (Fig. 6b). The lines in Fig. 6b are linear fits of the $H_{peak}(x)$ dependences. At $T=60$ K, the maximum in the $F_p(H)$ curves corresponds to $H=6.2$ T at $x=0.02$, $H=4.3$ T at $x=0.11$, and $H=3.8$ T at $x=0.25$. Apparently, the temperature decrease by 10 K causes the same shift of the H_{peak} peak position as the change in the x value from 0.02 to 0.25.

The dependence of the peak position on x in the range of $0.25 < x < 1$ is unknown and needs further investigations. In particular, the nonmonotonic dependence of H_{peak} on the x value was observed for the $Y_{1-x}Eu_xBa_2Cu_3O_7$ compound with $x > 0.5$ [13].

Sample treatment affects the sample porosity, the grain alignment and the grain size [36,37]. Structural differences of the samples influence on their critical current and may also shift the peak position H_{peak}. Since the investigated samples have the same disordered structure and the porosity does not affect the intragrain critical current density, we should consider an effect of different grain size on the peak field. Samples with grosser R have higher values of H_{irr}, because the irreversibility field determines the point in which $l_s(H)=R$ [26]. Provided $H_{peak}\approx0.2H_{irrc}$ (see Section 4.4), samples with grosser R have
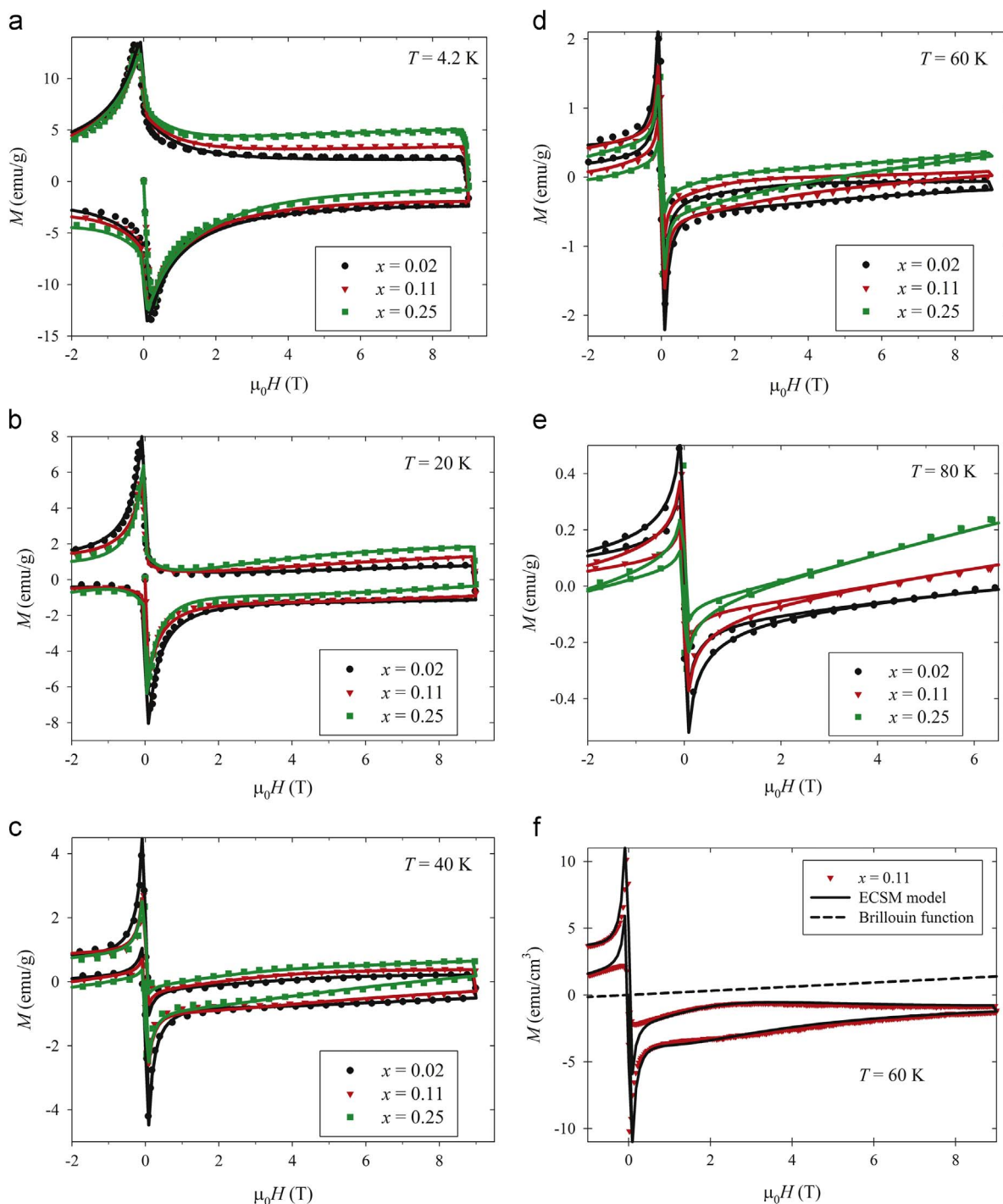
Fig. 4. Magnetization loops (a–e) at different temperatures and (f) magnetization loop without paramagnetic contribution for the sample with x=0.11 at T=60 K.

Table 1
Estimated parameters.

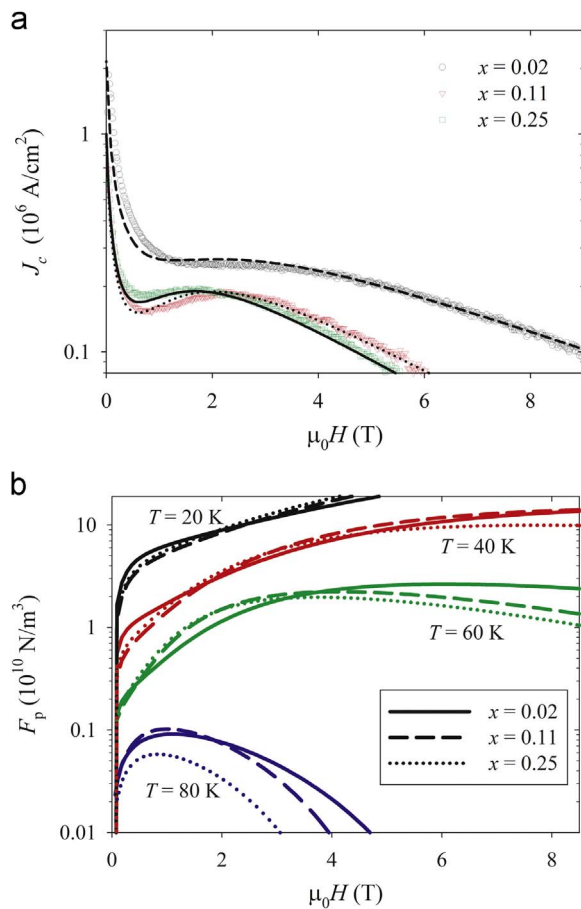| T, K	$J_c(0)$, 10^6 A/cm^2			A			$\mu_0 H_{tr}$, T		
	x=0.02	x=0.11	x=0.25	x=0.02	x=0.11	x=0.25	x=0.02	x=0.11	x=0.25
4.2	17	11	11	10	12	11	30	28	25
20	9.5	4.3	4.4	9.5	11.5	11	11.5	9.5	9
40	3.8	1.5	1.7	8	11	10.5	5.5	3.9	3.5
60	1.6	0.9	1	5	8	8	2.7	1.9	1.8
80	0.4	0.25	0.19	1.05	1.2	1.1	1	0.85	0.8

a

b

Fig. 5. Magnetic field dependences of (a) the critical current density and (b) pinning force density (semilog scale).

a

b

Fig. 6. Peak fields at different Nd contents x (semilog scale). Lines in Fig. 6b are linear fits.

higher H_{peak} also. Contrary to this, we observe the highest value of H_{peak} for the sample with $x=0.02$ having smaller R. This means that the Nd doping gives a prevalent influence that the grain size effect. The doping with rare-earth elements (RE) probably reduces characteristic fields of the order-disorder transition in the $Y_{1-x}RE_xBa_2Cu_3O_{7-\delta}$ compound. For undoped polycrystalline $YBa_2Cu_3O_{7-\delta}$ the peak effect is difficult to observe, in our opinion, because the second peak is very smooth and occurs in higher magnetic fields usually applied during measurements.

5. Conclusions

Polycrystalline $Y_{1-x}Nd_xBa_2Cu_3O_{7-\delta}$ ($x=0.02$, 0.11, and 0.25) superconductors were synthesized and characterized. The magnetization loops of the samples revealed the peak effect. It was found that substitution of Nd for Y does not improve the critical current, but tunes the second peak position. A noticeable decrease in the peak field and width results from doping with Nd. Analogously, the peak field, width, and height were found to decrease with increasing temperature.

The magnetization loops were successfully fitted using the extended critical state model. The peak effect was taken into account using the Boltzmann function describing the transition between the ordered and disordered states. The ECSM fitting using the Boltzmann function confirms that the peak effect is caused by the vortex lattice transition.
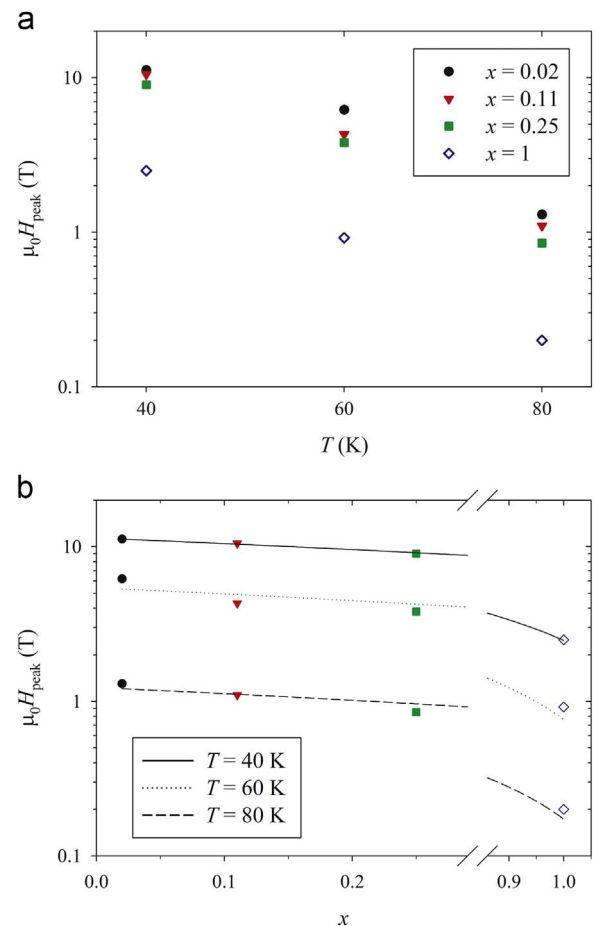
References

[1] B. Dam, J.M. Huijbregtse, F.C. Klaassen, R.C.F. van der Geest, G. Doornbos, J.H. Rector, A.M. Testa, S. Freisem, J.C. Martinez, B. Stäuble-Pümpin, R. Griessen, Origin of high critical currents in $YBa_2Cu_3O_{7-\delta}$ superconducting thin films, Nature 399 (1999) 439–442.

[2] N. Hari Babu, M. Kambara, E.S. Reddy, Y. Shi, D.A. Cardwell, Improved magnetic flux pinning in melt processed (Y, Nd)$Ba_2Cu_3O_{7-\delta}$ superconductor, Supercond. Sci. Technol. 18 (2005) S38–S42.

[3] K. Rogacki, B. Dabrowski, O. Chmaissem, Increase of critical currents and peak effect in Mo-substituted $YBa_2Cu_3O_7$, Phys. Rev. B 73 (2006) 224518.

[4] A.S. Mahmoud, G.J. Russell, M.R. Koblischka, N. Chikumoto, M. Murakami, Characterization of pinning in (Y, Nd)$Ba_2Cu_3O_{7-\delta}$ melt-textured superconductors, Physica C 415 (2004) 40–50.

[5] L. Krusin-Elbaum, L. Civale, V.M. Vinokur, F. Holtzberg, "Phase diagram" of the vortex-solid phase in Y-Ba-Cu-O crystals: a crossover from single-vortex (1D) to collective (3D) pinning regimes, Phys. Rev. Lett. 69 (1992) 2280–2283.

[6] M. Zehetmayer, How the vortex lattice of a superconductor becomes disordered: a study by scanning tunneling spectroscopy, Sci. Rep. 5 (2015) 9244.

[7] A.A. Gorbatsevich, Yu.V. Kopaev, I.V. Tokatly, Stratification and superconducting droplets in high-T_c superconductors, JETP Lett. 52 (1990) 95–98 [Pis'ma ZETF52

(1990) 736-739].

[8] D.A. Balaev, D.M. Gokhfeld, S.I. Popkov, K.A. Shaikhutdinov, L.A. Klinkova, L.N. Zherikhina, A.M. Tsvokhrebov, Increase in the magnetization loop width in the $Ba_{0.6}K_{0.4}BiO_3$ superconductor: possible manifestation of phase separation, J. Exp. Theor. Phys. 118 (2014) 104–110.

[9] P.J. Li, Z.H. Wang, H. Zhang, Y. Nie, Z. Bai, L. Qiu, S.Y. Ding, J. Gao, Effective pinning energy in Li-doped MTG-YBa$_2$Cu$_3$O$_y$ crystals, Supercond. Sci. Technol. 19 (2006) 392–396.

[10] T. Higuchi, S.I. Yoo, M. Murakami, Comparative study of critical current densities and flux pinning among a flux-grown NdBa$_2$Cu$_3$O$_y$ single crystal, melt-textured Nd-Ba-Cu-O, and Y-Ba-Cu-O bulks, Phys. Rev. B 59 (1999) 1514–1527.

[11] E. Altin, D.M. Gokhfeld, F. Kurt, M.E. Yakinci, Physical, electrical, transport and magnetic properties of Nd(Ba,Nd)$_{2.1}$Cu$_3$O$_{7-\delta}$ system, J. Mater. Sci.: Mater. Electron. 24 (2013) 5075–5084.

[12] E. Altin, D.M. Gokhfeld, S. Demirel, E. Oz, F. Kurt, S. Altin, M.E. Yakinci, Vortex pinning and magnetic peak effect in Eu(Eu,Ba)$_{2.125}$Cu$_3$O$_x$, J. Mater. Sci.: Mater. Electron. 25 (2014) 1466–1473.

[13] Y. Li, G.K. Perkins, A.D. Caplin, G. Cao, Q. Ma, L. Wei, Z.X. Zhao, Study of the pinning behaviour in yttrium-doped Eu-123 superconductors, Supercond. Sci. Technol. 13 (2000) 1029–1034.

[14] Y. Feng, A.K. Pradhan, Y. Zhao, Y. Wu, N. Koshizuka, L. Zhou, Influence of Ho substitution for Y on flux pinning in melt-processed YBCO superconductors, Physica C 357–360 (2001) 799–802.

[15] P.N. Barnes, J.W. Kell, B.C. Harrison, T.J. Haugan, C.V. Varanasi, M. Rane, F. Ramos, Minute doping with deleterious rare earths in YBa$_2$Cu$_3$O$_{7-\delta}$ films for flux pinning enhancements, Appl. Phys. Lett. 89 (2006) 012503.

[16] M.I. Petrov, Yu.S. Gokhfeld, D.A. Balaev, S.I. Popkov, A.A. Dubrovskiy, D.M. Gokhfeld, K.A. Shaykhutdinov, Pinning enhancement by heterovalent substitution in Y$_{1-x}$RE$_x$Ba$_2$Cu$_3$O$_{7-\delta}$, Supercond. Sci. Technol. 21 (2008) 085015.

[17] X.Q. Xu, Y.Q. Cai, C.X. Yang, X. Yao, S. Xu, A. Kortyka, R. Puzniak, Effect of Pr doping on the growth and superconducting properties of (Y$_{1-x}$Pr$_x$)Ba$_2$Cu$_3$O$_{7-\delta}$, Supercond. Sci. Technol. 22 (2009) 015001.

[18] A. Öztürk, İ. Düzgün, S. Çelebi, The effect of partial Lu doping on magnetic behaviour of YBCO (123) superconductors, J. Alloy. Compd. 495 (2010) 104–107.

[19] M.H. Wahid, Z. Zainal, I. Hamadneh, K.B. Tan, S.A. Halim, A.M. Rosli, E.S. Alaghbari, M.F. Nazarudin, E.F. Kadri, Phase formation by REBa$_2$Cu$_3$O$_{7-\delta}$ (RE: Y$_{0.5}$Gd$_{0.5}$, Y$_{0.5}$Nd$_{0.5}$, Nd$_{0.5}$Gd$_{0.5}$) superconductors from nanopowders synthesised via co-precipitation, Ceram. Int. 38 (2012) 1187–1193.

[20] D.N. Matthews, J.W. Cochrane, G.J. Russell, Melt-textured growth and characterisation of a (Nd/Y)Ba$_2$Cu$_3$O$_{7-\delta}$ composite superconductor with very high critical current density, Physica C 249 (1995) 255–261.

[21] N.K. Saritekin, M. Oz, C. Terzioglu, O. Gorur, G. Yildirim, Significant development on pinning of vortices in Y-123 superconductor with homovalent Ba/Nd substitution, J. Mater. Sci.: Mater. Electron. 27 (2016) 6992–7003.

[22] X. Yao, E. Goodilin, Y. Yamada, H. Sato, Y. Shiohara, Crystal growth and

superconductivity of Y$_{1-x}$Nd$_x$Ba$_2$Cu$_3$O$_{7-\delta}$ solid solutions, Appl. Supercond. 6 (1998) 175–183.

[23] D.M. Gokhfeld, S.V. Semenov, D.A. Balaev, I.S. Yakimov, A.A. Dubrovskiy, K. Yu, Terentyev, A.L. Freydman, A.A. Krasikov, M.I. Petrov, Establishing of peak effect in YBCO by Nd substitution, JMMM (2017). http://dx.doi.org/10.1016/j.jmmm.2016.12.089.

[24] S. Çelebi, A. Öztürk, U. Çevik, Magnetic responses of a high-T_c semi-reversible YBCO superconductor, J. Alloy. Compd. 288 (1999) 249–254.

[25] D.M. Gokhfeld, D.A. Balaev, M.I. Petrov, S.I. Popkov, K.A. Shaykhutdinov, V.V. Valkov, Magnetization asymmetry of type-II superconductors in high magnetic fields, J. Appl. Phys. 109 (2011) 033904.

[26] D.M. Gokhfeld, An extended critical state model: asymmetric magnetization loops and field dependence of the critical current of superconductors, Phys. Solid State 56 (2014) 2380–2386.

[27] Y.I. Yakimov, L.A. Solovyov, A.N. Zaloga, I.S. Yakimov, DDMSuite – a powder diffraction full-profile analysis system, Acta Cryst. A 66 (2010) S316.

[28] K.A. Shaikhutdinov, D.A. Balaev, S.I. Popkov, M.I. Petrov, Thermally activated dissipation in a novel foamed Bi-based oxide superconductor in magnetic fields, Supercond. Sci. Technol. 20 (2007) 491–494.

[29] D.A. Balaev, A.G. Prus, K.A. Shaykhutdinov, D.M. Gokhfeld, M.I. Petrov, Study of dependence upon the magnetic field and transport current of the magnetoresistive effect in YBCO-based bulk composites, Supercond. Sci. Technol. 20 (2007) 495–499.

[30] D.A. Balaev, A.A. Bykov, S.V. Semenov, S.I. Popkov, A.A. Dubrovskii, K.A. Shaykhutdinov, M.I. Petrov, General regularities of magnetoresistive effects in the polycrystalline yttrium and bismuth high-temperature superconductor systems, Phys. Solid State 53 (2011) 922–932.

[31] C.P. Bean, Magnetization of hard superconductors, Phys. Rev. Lett. 8 (1962) 250–253.

[32] D.M. Gokhfeld, Critical current density and trapped field in HTS with asymmetric magnetization loops, J. Phys. Conf. Ser. 695 (2016) 012008.

[33] L. Burlachkov, Magnetic relaxation over the Bean-Livingston surface barrier, Phys. Rev. B 47 (1993) 8056–8064.

[34] D.M. Gokhfeld, Secondary peak on asymmetric magnetization loop of type-II superconductors, J. Supercond. Nov. Magn. 26 (2013) 281–283.

[35] T.V. Sukhareva, V.A. Finkel, Phase transition in the vortex structure of granular YBa$_2$Cu$_3$O$_{7-\delta}$ HTSCs in weak magnetic fields, J. Exp. Theor. Phys. 107 (2008) 787–793.

[36] M.E. Yakinci, M.A. Aksan, Y. Balci, S. Altin, Effects of thickness on the grain alignment and J_c properties of (Hg$_{0.8}$Re$_{0.2}$)Ba$_2$Ca$_2$Cu$_3$O$_x$ superconductor thick films, Physica C 460–462 (2007) 1386–1387.

[37] Z.D. Yakinci, D.M. Gokhfeld, E. Altin, F. Kurt, S. Altin, S. Demirel, M.A. Aksan, M.E. Yakinci, J_c enhancement and flux pinning of Se substituted YBCO compound, Mater. Sci.: Mater. Electron. 24 (2013) 4790–4797.